This project has received funding from the European Union's Horizon 2020 research and innovation programme under Grant Agreement No. 837733.

COZMOS

EU-project Horizon 2020

Efficient CO_2 conversion over multisite Zeolite-Metal nanocatalysts to fuel and OlefinS

Grant Agreement No. 837733

Deliverable Report

Deliverable ID	D.1.16		
Deliverable name	Report on catalyst synthesis and testing		
Lead beneficiary	University of Oslo		
Contributors	KAUST, UniTo, TOPSOE, UiO		
Due date Annex I	M45		
Date of final version	10.02.2023		
Dissemination level	Public		
Document approval	Unni Olsbye	10.02.2023	

Executive Summary

In this public report, we present the main results obtained with the best identified tandem system for the direct conversion of CO_2 into propane, from the initial synthesis at lab-scale to the catalyst upscaling. The $PdZn/ZrO_2$ + SAPO-34 catalyst combination was found to provide the highest combined CO_2 conversion (40%) and propane selectivity (50%, with 20% CO, 6% C_1, 13% C_2, 10% C_4, and 1% C_5), achieving two of the three key performance indicators (KPIs) defined in the COZMOS project for catalyst performance.

This catalyst combination was selected as our 1st generation catalyst in the project, and different strategies for catalyst production upscaling have been investigated. The physical mixture of the upscaled version of $PdZn/ZrO_2$ and SAPO-34 achieved 90% of the catalytic performance previously observed for the lab-scale catalyst, also meeting the established KPI. Otherwise, the formulation of technical catalyst in tablet or extrudate shapes demonstrated the migration of Zn from the ZrO_2 matrix to the Al-containing binder and the SAPO-34 function. The significant loss of activity in these cases suggested the impracticality of using these shapes for this catalyst combination.

The upscaled catalyst mixture was extensively tested for tandem CO_2 hydrogenation and a detailed kinetic model was developed. The versatility of the models allowed the prediction of product distribution using different reaction (temperature, pressure and space velocity) and operation conditions (CO_2 feeds, CO feeds and CO_2/CO feeds).

These kinetic rate expressions were communicated from WP1 (*catalyst development*) to WP2 (*plant design*), WP3 (*pilot-plant testing*) and WP4 (*Life Cycle Assessment*), enabling the project's industrial partners to design an industrial plant and perform techno-economic and life cycle assessments (TEA and LCA, WP2 and WP4, respectively). Moreover, this catalyst combination is currently in pilot-plant testing within the COZMOS activities of WP3.

Table of Contents

1 Introduction

The COZMOS project targets a process to produce C_3 hydrocarbons, propane and propene, from CO_2-containing industrial effluents. When proposing this project (TRL3), the best, combined C_2-C_4 yield reported in the open literature from a CO_2/H_2 feed over a tandem catalyst was 1.5 %.[1] In comparison, the best C_3 yield obtained in COZMOS to date is 20%, more than an order of magnitude higher than the starting point. The successful project achievements build on the strong materials, catalysis and process expertise gathered in the COZMOS team, combined with extensive synthesis, characterization, and testing efforts. The COZMOS project targets a process to produce C_3 hydrocarbons, including propane and propene. With the first generation catalyst, PdZn/ZrO_2 + H-SAPO-34, we observed a 100% selectivity to paraffins due to the outstanding hydrogenation activity offered by PdZn alloy (also highest CO_2 conversions found to date). However, the search for olefins as primary products was one reason to investigate other active catalysts as our 2nd generation catalyst (not reported here).

In previous public reports, we detailed the different approaches used during the extent of the project to achieve the Key Performance Indicators (KPIs) defined for the project. In the public D.1.6 deliverable, the preparation and characterization of different zeolites/zeotypes were discussed. Moreover, their activity for methanol conversion into hydrocarbons was evaluated, as well as their performance on tandem reaction as part of bifunctional systems. Some combinations of mixed oxides (active materials for CO_2 hydrogenation to methanol) with these zeolites were reported as potential catalyst candidates, among which we highlighted: $ZnCeZrO_x$ + H-RUB-13, $GaZrO_x$ + H-SSZ-13, ZnO:ZrO_2 + H-ZSM-5 and PdZn/ZrO_2 + H-SAPO-34.

In the public D.1.5 report, hybrid catalytic systems were presented, where the two active functions (for CO_2 and methanol conversion, respectively) are in close proximity. Surface organometallic chemistry of unmodified zeolites, impregnated zeolites and modified zeolites provided these materials with the bifunctional sites able to convert CO_2 directly to hydrocarbons. The main results obtained with PdZn hybrid systems on H-ZSM-5, H-SAPO-34 and H-SAPO-34 were discussed in D.1.5, evaluating the main physicochemical properties of these materials and their activity for the tandem CO_2 hydrogenation.

This report presents an overview of the synthesis and testing activities for the best identified bifunctional system for propane production during M1-M45 of the COZMOS project. This catalyst combination, PdZn/ZrO_2 + SAPO-34, was selected as first generation catalyst among an intensive series of tested candidates.

[1] P. Gao et al.; Direct conversion of CO_2 into liquid fuels with high selectivity over a bifunctional catalyst. *Nature Chemistry*, **2017**, 9, 1019–1024.

2 First generation catalyst: $PdZn/ZrO_2$ + SAPO-34

2.1 Catalyst synthesis and characterization

The $PdZn/ZrO_2$ catalyst was obtained by a colloidal impregnation method. Briefly, 5 g L^{-1} of $Pd(CH_3COO)_2$ was dissolved in DMF and 20 g L^{-1} $Zn(CH_3COO)_2$ dissolved in ethylene glycol were prepared. Eight grams of PVP was added to 80 mL of the Zn precursor solution and heated to 80 °C to obtain a clear yellow solution. Fifty milliliters of the Pd precursor solution was added to the clear yellow zinc/PVP solution amidst stirring and heated to 100 °C under reflux for 2 h. The colloidal mixture was cooled, centrifuged, and washed with acetone and then dispersed in ethanol. The dispersed colloidal mixture in ethanol was added to 6 g of $Zr(OH)_4$ powder and stirred for 20 h at room temperature. The resulting mixture was oven-dried and calcined at 500 °C for 3 h. SAPO-34 (SiO_2/Al_2O_3 = 0.5) was purchased from ACS materials. It was dried at 120 °C for 12 h and calcined at 550 °C for 2 h prior to testing. The multifunctional $PdZn/ ZrO_2$ + SAPO-34 catalysts was prepared by mortar mixing of both components with a 1:1 mass ratio.

The bifunctional catalyst was characterized using several techniques to elucidate the nature of the active sites for CO_2 hydrogenation. X-ray absorption spectroscopy (XAS) was performed on the $PdZn/ZrO_2$ catalyst in an element-selective way, and revealed Pd- and Zn-containing species formed in a model multifunctional system, in its as-prepared state and upon activation. The XAS spectra reported in **Figure 1** show how electronic and structural features of both Pd and Zn change considerably when the catalyst is subjected to the activation treatment. Indeed, both XANES (main panels) and EXAFS spectra (insets) show substantial modifications at high temperature in the presence of H_2. Considering the Pd K edge, the as-prepared catalyst (**Figure 1a**) presents the typical XANES (edge position, postedge resonances) and EXAFS (Pd−O bond in first coordination shell) features of a reference PdO sample. During activation (**Figure 1b**, from ca. 50 °C up to ca. 200 °C) Pd(II)-to-Pd(0), reduction is underlined by: (i) shift of the absorption edge position to lower energy; (ii) rapid change of the oscillation in the XANES from PdO-like to those resembling metallic Pd (**Figure 1a, b** light gray line), and; (iii) intensity loss of the Pd−O first coordination shell in the phase-uncorrected EXAFS (inset **Figure 1b**) and shift to lower R values of the Pd−Pd second coordination shell. As the temperature rises (300 °C), the oscillations in the XANES get flatter and EXAFS evolves into a single broad peak around 2.15 Å in the phase-uncorrected spectrum (**Figure 1b** red curve). These features were already observed and well reported in the case of other PdZn systems and ascribed to the formation of β1-PdZn alloy.[2,3]

[2] M.W. Tew et al., Formation and Characterization of PdZn Alloy: A Very Selective Catalyst for Alkyne Semihydrogenation. *J. Phys. Chem. C*, **2011**, 115, 8457−8465.
[3] M. Gentzen et al., Supported Intermetallic PdZn Nanoparticles as Bifunctional Catalysts for the Direct Synthesis of Dimethyl Ether from CO-Rich Synthesis Gas. *Angew. Chem., Int. Ed*. **2019**, 58, 15655−15659.

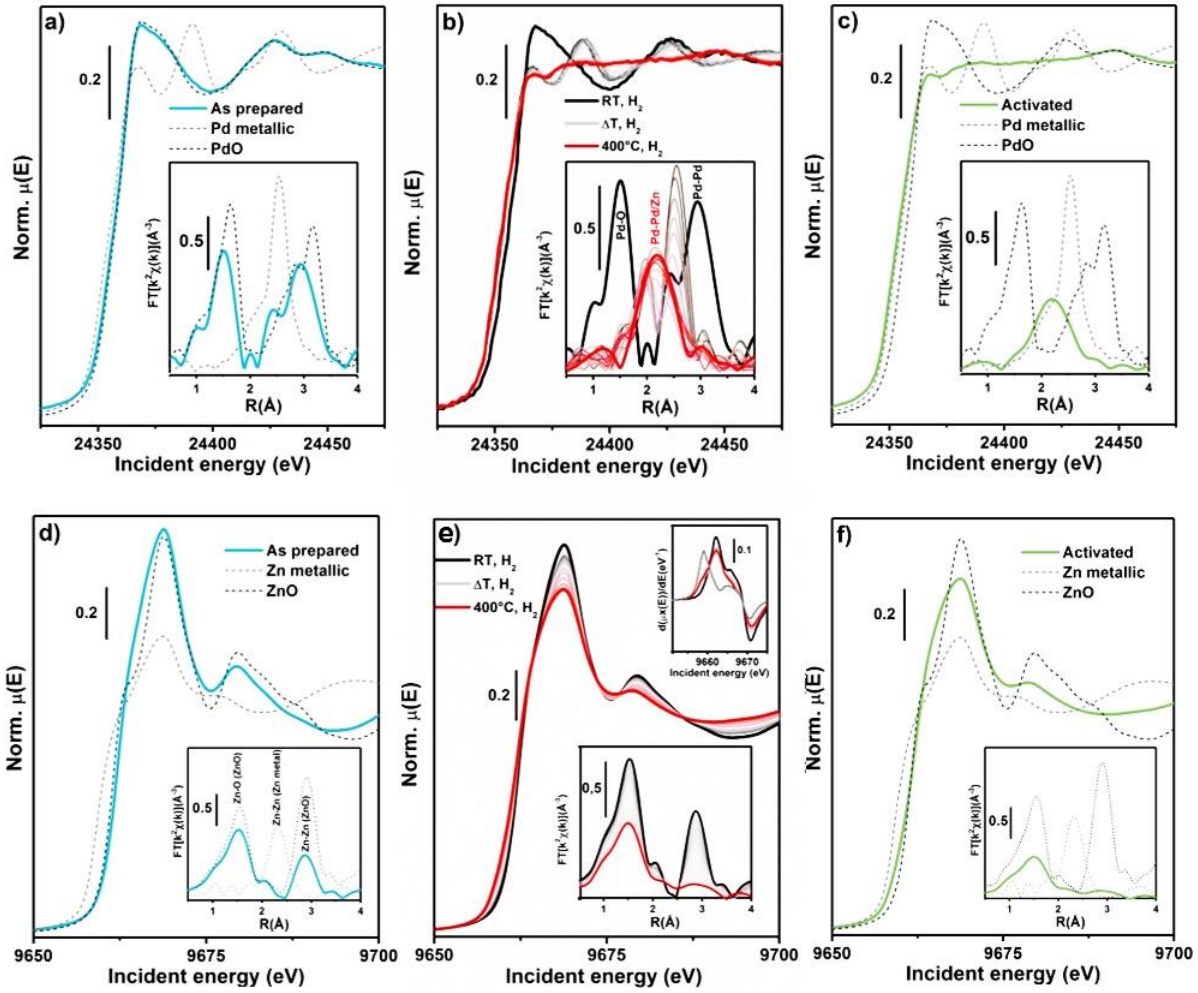

Figure 1. Pd K-edge, Zn K-edge XANES (main panels), and EXAFS (insets) spectra of $PdZn/ZrO_2$+ZSM-5 catalyst. XAS spectra for relevant reference compounds are also reported as dashed lines. (a) Pd K-edge for as prepared catalyst. (b) Pd K-edge for catalyst during activation (RT-400 °C) under H_2 gas flow. (c) Pd K-edge for catalyst after activation at 400 °C under H_2 atmosphere. (d) Zn K-edge for as prepared catalyst. (e) Zn K-edge for catalyst during activation (RT-400 °C) under a H_2 gas flow. Top right inset: first derivative of the XANES spectra for as prepared catalyst (black), activated catalyst (red), reference Zn(0) metal foil (light gray). (f) Zn K-edge for catalyst after activation at 400 °C under a H_2 gas flow. For clarity of comparison, the Pd metallic foil EXAFS signal was rescaled by a factor of 1/2. The EXAFS spectra reported in the bottom insets have been obtained by transforming the corresponding k2χ(k) EXAFS function in the 2.5−11.0 $Å^{-1}$ range. Reproduced from [4].

Moving to the Zn K-edge, the as-prepared catalyst (**Figure 1d**) essentially presents the same XANES and EXAFS features of a reference ZnO sample. A careful observation of the EXAFS data unveils a lower intensity of the second shell peak in the catalyst with respect to the reference oxide (inset **Figure 1d**), indicating a higher concentration of defects in the former. From the Zn perspective, the activation protocol causes (i) a pronounced decrease of the signal intensity in both the XANES and EXAFS region and (ii) a subtle red-shift of the edge energy position, better observed from the growth of a shoulder at low energy values in the XANES

[4] Ramirez et al., Multifunctional Catalyst Combination for the Direct Conversion of CO_2 to Propane. *JACS Au*, **2021**, 1, 1719–1732. DOI: 10.1021/jacsau.1c00302

first derivative, matching the first maximum for Zn(0) metal foil (top right inset **Figure 1e**). Zn species are present in the activated sample (**Figure 1f**), and therefore they dominantly occur as a highly defective ZnO phase with a minor Zn(0) contribution ascribable to the fraction of Zn taking part to the formation of PdZn alloy. Moreover, in the physical mixture of PdZn/ZrO_2 + zeolites/zeotypes, fingerprints of Zn-exchanged zeolite were not observed,[5] suggesting that impregnating Pd and Zn over ZrO_2 stabilizes the former atoms, avoiding their further diffusion into the zeolite component.

To confirm this observation, *in-situ* high-angle annular dark-field transmission electron microscopy (HAADF-TEM) experiments were carried out for the as-made PdZn/ZrO_2 catalyst (**Figure 2a**), after reduction treatment in H_2 (**Figure 2b**) and after CO_2 + H_2 treatment (**Figure 2c**). During H_2 activation, the small PdO nanoparticles merge and reduce into 10 to 30 nm metallic nanoparticles (**Figure 2b**). The elemental composition as revealed by STEM-EDS shows clearly the formation of a PdZn alloy at that stage. CO_2 hydrogenation is also confirmed to induce the formation of the ZnO shell on the surface of the PdZn alloy (**Figures 2b** and **2c**), which was further established by multiple observations in several areas of the sample.

[5] Pinilla-Herrero et al., High Zn/Al Ratios Enhance Dehydrogenation vs Hydrogen Transfer Reactions of Zn-ZSM-5 Catalytic Systems in Methanol Conversion to Aromatics. *J. Catal*. **2018**, 362, 146−163.

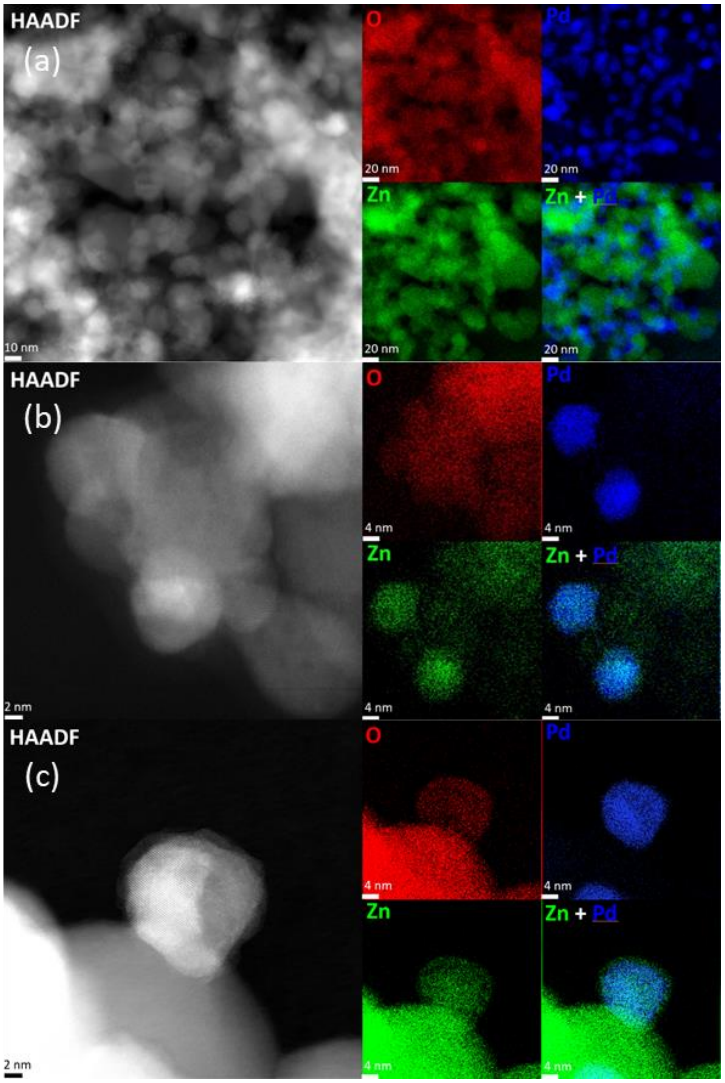

Figure 2. HAADF-STEM imaging of (a) as-synthesized $PdZn/ZrO_2$ catalyst, (b) PdZn alloy nanoparticle after H_2 activation handled without air exposure and (c) PdZn alloy nanoparticle after $CO_2 + H_2$ treatment handled without air exposure and related elemental maps built with K_α emission lines provided by Pd, O, and Zn atoms. Reproduced from [4].

2.2 Catalytic testing

Catalytic tests were carried out in a 16 channel Flowrence set-up from Avantium. Samples of stand-alone $PdZn/ZrO_2$ and mixtures of $PdZn/ZrO_2$ + SAPO-34 were placed in the fixed bed reactors. Typically, both functions were pelletized together in a 1/1 ratio, and then sieved to a particle size 150−250 μm. The mixed feed had 22.5 vol % of CO_2, 72.5 vol % of H_2, and 5% of He as internal standard. One of the 16 channels was always used without catalyst as blank. Prior to feeding the reaction mixture all samples were pretreated *in situ* under a pure H_2 flow for 4 h at 400 °C. The tubes were then pressurized to 30 bar using a membrane- based pressure controller. Operation conditions were ranged between 250 and 350 °C, 30−50 bar and Gas Hourly Space Velocity (GHSV) 1500−12000 mL g^{-1} h^{-1}. Reaction products were analyzed online in a gas chromatograph. The GC is an Agilent 7890B with three detectors, a TCD and 2 FIDs. TCD is equipped with 2 Haysep precolumns and a MS5A, where He, H_2, CH_4, CO_2, and CO are separated. FIDs are equipped with Gaspro and Innowax columns. Gaspro separates C_1-

C_8 hydrocarbons and DME. Innowax separates oxygenates and aromatics. Conversion and selectivity were calculated in C basis.

Figure 3a shows the evolution with GHSV of CO_2 conversion, CO selectivity and propane selectivity as the main hydrocarbon product obtained at 30, 40 and 50 bar total pressure. CO_2 conversion increases with decreasing GHSV and increasing pressure. However, CO selectivity also decreases with GSHV, reaching a minimum value of 25% at 50 bar and 1500 mL g^{-1} h^{-1}. These data may suggest that CO-involving reactions play a key role using the $PdZn/ZrO_2$ + SAPO-34 system, because of a limitation in its formation or a consumption of the formed CO to produce more methanol. Moreover, from the data at 50 bar and 1500 mL g^{-1} h^{-1}, a total selectivity to propane higher than 50% can be observed, with a CO_2 conversion close to 40% and only 25% of CO selectivity. Hydrocarbon distribution at 50 bar is depicted in **Figure 3b**, where the predominance of paraffins in the product stream is observed due to the Pd hydrogenating effect. In all cases, propane is the main hydrocarbon product, also increasing its yield at the lowest GHSV tested.

Apart from the evident role of CO in CO_2 hydrogenation, the reactivity of CO over this catalyst will be also relevant for industrial conditions, where most of the unreacted CO_2 + CO needs to be recirculated to increase the overall conversion of the process. To shed light on the CO role, additional experiments with both CO_2 and CO feeds were performed comparing the $PdZn/ZrO_2$ + SAPO-34 mixed system, the stand-alone $PdZn/ZrO_2$ catalyst and the multifunctional system in dual bed configuration. The results are summarized in **Figure 3c** and **3d**. Considering first the CO_2 feed (**Figure 3c**), the rather stable CO_2 conversion, and the huge decrease in CO selectivity (from 95% to 35%), only observed when mixing $PdZn/ZrO_2$ with SAPO-34, suggests a lower CO formation rate in the presence of SAPO-34. The similar CO selectivity with similar CO_2 conversion in the dual bed setup confirms that, indeed, the intimate mixture of both components is needed to displace equilibrium. CO conversion (**Figure 3d**) is substantially lower than that of CO_2, but with higher methanol selectivity compared to CO_2 over the $PdZn/ZrO_2$ alone. This is in line with process thermodynamics (the lower the conversion, the higher the MeOH selectivity) but also suggests that CO limits the rate of the reaction. CO conversion is also increased in the mixed bed configuration, indicating the clear effect of CO and water-gas shift reaction in the mixed bed configuration.

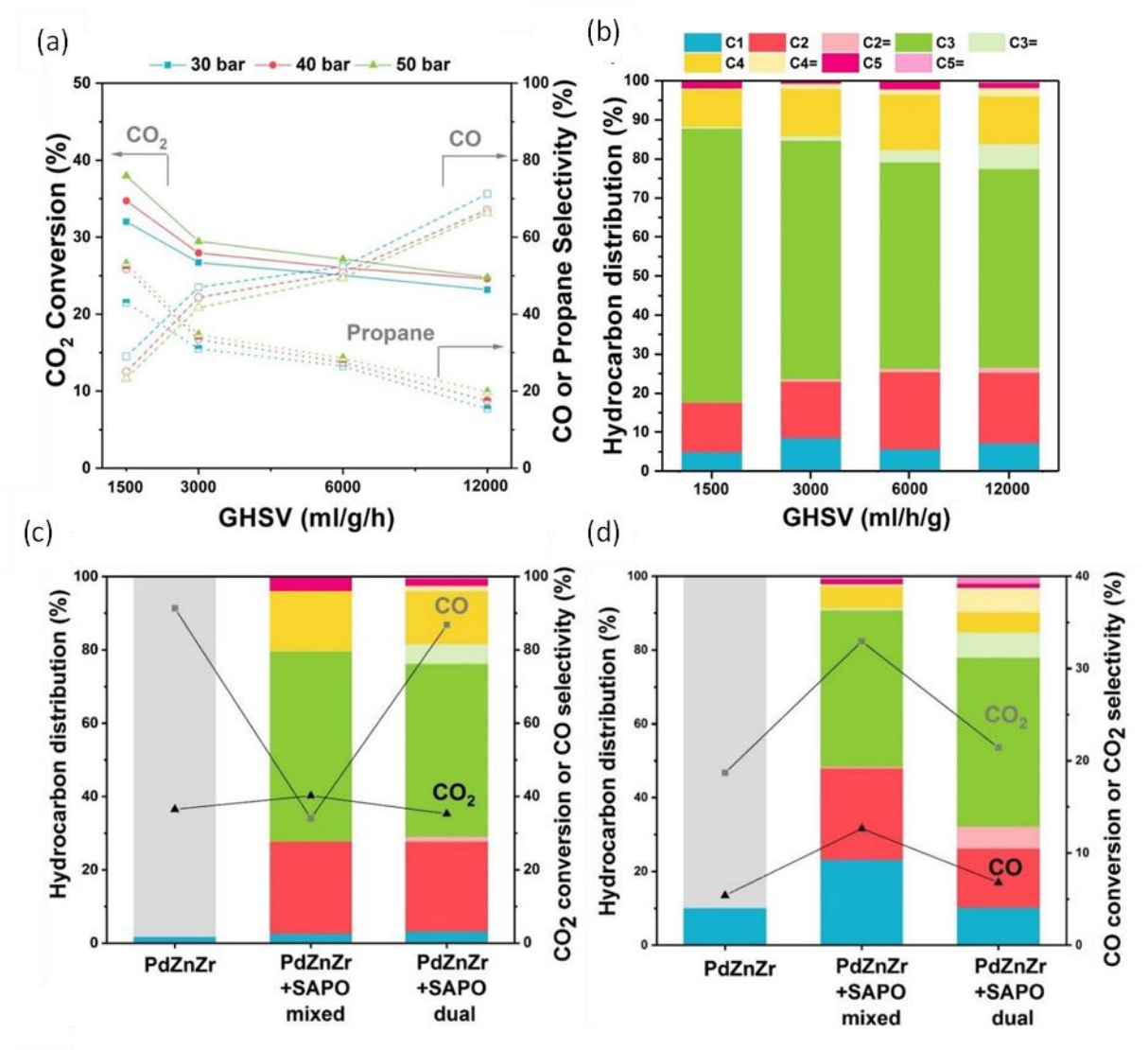

Figure 3. (a) CO_2 conversion (filled symbols) and CO (empty symbols) or propane (half-empty symbols) selectivity for the $PdZn/ZrO_2$ + SAPO-34 system at different space velocities and pressures. 350 °C, H_2/CO_2 = 3. MeOH selectivity was lower than 1% at all conditions. (b) Detailed hydrocarbon distribution (CO free) of the $PdZn/ZrO_2$+SAPO-34 combined system for the CO_2 conversion to hydrocarbons at different space velocities. CO_2:H_2 1:3, 350 °C, 50 bar. Catalytic performance of the $PdZn/ZrO_2$ catalyst and the $PdZn/ZrO_2$ + SAPO-34 combined system: (c) CO_2 and (d) CO conversion to hydrocarbons. CO_x:H_2 1:3, 350 °C, 30 bar, 3000 mL g^{-1} h^{-1}. Reproduced from [4].

3 Synthesis optimization and upscaling

3.1 Protocols of synthesis upscaling

The first version of the most active $PdZn/ZrO_2$ catalyst for CO_2 hydrogenation was synthesized by a colloidal impregnation method. Despite the advantages of this methodology to control catalyst composition and active sites location, the complexity of experimental protocols hindered an optimized upscaling of this procedure. For that reason, we first investigated a simplified protocol based on incipient wetness impregnation for the preparation of the catalyst.

Briefly, the $PdZn/ZrO_2$ catalyst was prepared by adding 10 g of Zirconium(IV) oxide (Merck) to a solution of 3.4 g Zn $(NO_3)\cdot 6\ H_2O$ (Merck) and 0.33 g $Pd(NO_3)_2$ (Merck) in 7 ml of water. The mixture was stirred for about 15 min, and then evaporated under stirring at 65 ºC. Afterwards, the material was dried at 200 °C for 1 h and calcined at 500 °C for 5 h. The calcined catalyst was reduced for 1 h in hydrogen at 400 °C (ramp 5 °C min^{-1}), to form the active PdZn alloy species, and finally passivated at room temperature in 1% O_2 in N_2 to stabilize the active function.

Aiming at the preparation of technical catalysts for industrial application, tablets and extrudates of this $PdZn/ZrO_2$ version were also synthesized. The calcined precursor was mixed with commercial SAPO-34 (China Catalyst Holding Co.) and alumina binder and pelletized to form a robust catalyst body (PZZ-ox-tab). The SAPO-34 was previously calcined at 475 ºC for 2 hours to remove template and carbonaceous residues in the as-received material. Final composition of the tablets was approx. 45:45:10 wt% of $PdZn/ZrO_2$, SAPO-34 and Al_2O_3 respectively. Extrudates were prepared by mixing the calcined catalyst precursor with the SAPO-34 and alumina binder with water to form a paste. The paste was extruded on a piston extruder, dried and calcined 5 hours at 500 ºC to obtain a catalyst, PZZ-ox-ext, with approx. 30:30:40 wt% of $PdZn/ZrO_2$, SAPO-34 and Al_2O_3, respectively. For both tablets and extrudates a dual strategy was pursued, using calcined (PZZ-ox) and reduced (PZZ-red) precursors, respectively. Reduction of the (calcined) $PdZn/ZrO_2$ precursor was performed in a flow of hydrogen (2 vol%) in Ar at 400ºC for 20 hours. The final catalysts with reduced precursors were subjected to final calcination as described above to produce PZZ-red-ext (extrudates) and PZZ-red-tab (tablets). A summary of all synthesized iterations of this catalyst combination is illustrated in **Table 1**.

Table 1. Summary of the $PdZn/ZrO_2$ + SAPO-34 catalysts synthesized and tested during the COZMOS project

#	Nomenclature	Formulation	Comment
1	$PdZn/ZrO_2$ + SAPO-34	Physical mixture	First tested catalyst synthesized by colloidal impregnation
2	PZZ + SAPO-34	Physical mixture	Optimized synthesis by incipient wetness impregnation
3	PZZ-tab + SAPO-34-ext	Physical mixture (PZZ in tablets, SAPO-34 in extrudates)	Under investigation at pilot plant (TRL5)
4	PZZ-tab (45:45:10)	Tablet of both functions	Tested at lab scale
5	PZZ-ext (30:30:40)	Extrudates of both functions	Tested at lab scale

3.2 Catalytic activity of the upscaled catalyst

The catalytic performance for the tandem CO_2 hydrogenation of these series of upscaled catalyst is shown in **Figure 4**. For the sake of comparison, we have also included the results obtained with the standalone $PdZn/ZrO_2$ catalyst obtained by incipient wetness impregnation. These two scaled up standalone $PdZn/ZrO_2$ mixed oxides (PZZ) do produce methanol and CO as main products, in line with the laboratory-scale $PdZn/ZrO_2$ catalyst (**Figure 3**). Nevertheless, the reduced catalyst (*ex-situ* after the synthesis), performed ostensibly better, with similar conversion and more than double methanol selectivity due to the decrease in CO production. The mixture of this catalyst with the SAPO-34 (PZZ-red + SAPO-34) performed very closely to the original version at lab scale. At 350 °C, 30 bar, 6000 mL g^{-1} h^{-1}, PZZ + SAPO-34 showed a CO_2 conversion of 27% with CO selectivity of 65% (**Figure 4a**), while the first version of this catalyst ($PdZn/ZrO_2$ + SAPO-34) showed 26% CO_2 conversion with CO selectivity of 60% (**Figure 3a**). Despite the slightly higher selectivity to CO, this catalyst combination meets the 90% KPI defined at the beginning of the COZMOS project.

As observed before, this physical mixture of the functions boosts CO_2 conversion by converting *in situ* the produced methanol to hydrocarbons. CO selectivity is significantly reduced (from ca. 86 to 65%) due to a shift in the reaction network equilibria and methane selectivity is also minimized. Otherwise, this increase in CO_2 conversion was not observed for the technical catalysts. Please note that the composition of each technical catalyst is slightly different so a small decrease in CO_2 conversion could be expected from physical mixture to tablets and extrudates (**Table 1**). Looking at the tablet technical catalysts, both PZZ-ox-tab and PZZ-red-tab catalysts are able to yield propane as the main hydrocarbon product. Besides, PZZ-red-tab outperformed its non-reduced counterpart PZZ-ox-tab with double propane selectivity, as one should expect after the comparison of the mixed oxides PZZ-ox and PZZ-red. The catalytic performance of PZZ-red-tab is also very stable during the 72 hours studied (see **Figure 4b**). Nevertheless, the catalytic performance of this technical catalyst is much inferior to the physical mixture, with a CO_2 conversion of only ca. 14% and a high methane selectivity (10%). This loss of activity becomes even worse when the technical catalyst is shaped into an extrudate form (PZZ-ox-ext and PZZ-red-ext). The catalytic activity is lost, without observing any propane in the product effluent. Surprisingly, the catalyst converts CO_2 into methanol (with some DME) and methane as the main byproduct. This result suggests a very likely poisoning of the SAPO-34 sites during catalyst shaping and potential modifications of the hydrogenation function, which is still able to hydrogenate CO_2.

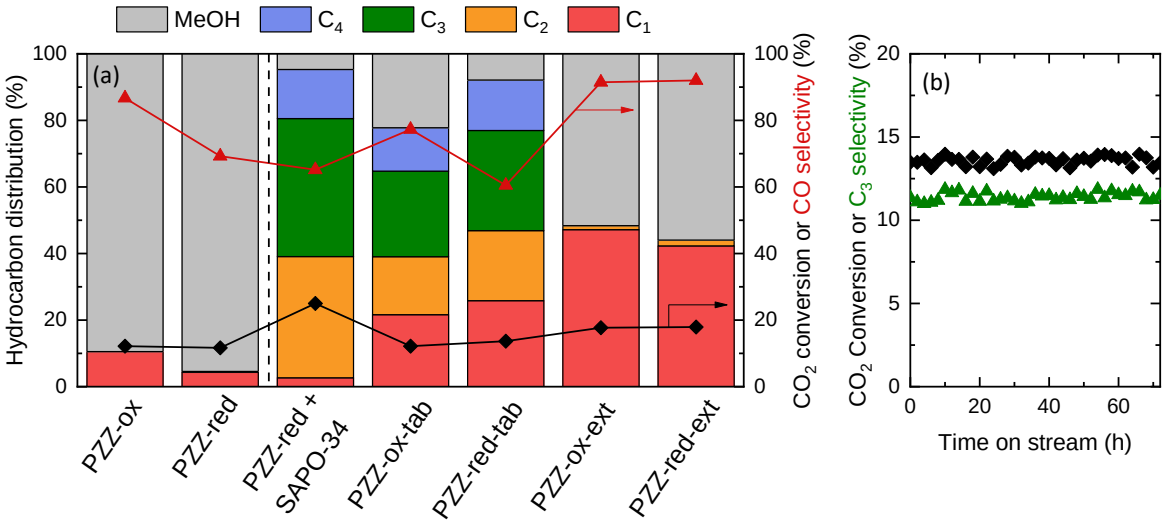

Figure 4. (a) CO_2 conversion and hydrocarbon distribution for the different technical catalysts and (b) evolution with time on stream of CO_2 conversion and C_3 selectivity for the PZZ-red-tab catalyst. Reaction conditions: 350 °C, 30 bar, 6000 mL g^{-1} h^{-1}, CO_2:H_2 1:3. Reproduced from [6].

The main hypothesis for this loss of SAPO-34 activity was a migration of Zn from the oxide to the Al matrix and SAPO-34. XAS Zn k-edge results of tablets suggested the absence of PdZn-related energy shift and rise of shoulder in the lower-energy region of the spectrum. Moreover, extrudates showed similar Zn K-edge spectra to those characteristic of Zn-aluminates. Since Zn migration was not observed when mixing $PdZn/ZrO_2$ with SAPO-34, extrudate and tablet spectra suggested as Zn aluminates are most likely formed when contacting the catalyst with an Al_2O_3-based binder, which was more clearly observed in the case of extrudates. This result is consistent with the observed activity loss (**Figure 4a**), more pronounced in the case of extrudates (no hydrocarbons in the effluent).

Elemental mapping performed by scanning electron microcopy (SEM) also demonstrate the presence of Zn in the SAPO-34 for the extruded catalyst. **Figure 5** shows element concentration profiles along lines across the shaped extrudates. The profiles indicate that Zn tends to migrate onto both the alumina binder (primarily in extrudates) and the SAPO-34 phases whereas Pd appears to adsorb strongly on the ZrO_2 support. This result is in line with ZnO loss observed by XAS and PXRD (Figures not shown). For the sake of completeness, it should be mentioned that no differences between the oxidized and reduced forms of the precursors are observed and Zn migration seems to be independent of the precursor pretreatments.

[6] Ticali et al., From Lab to Technical CO_2 Hydrogenation Catalysts: Understanding PdZn Decomposition. *ACS Appl. Mater. Interfaces,* **2023**, DOI: 10.1021/acsami.2c19357 A

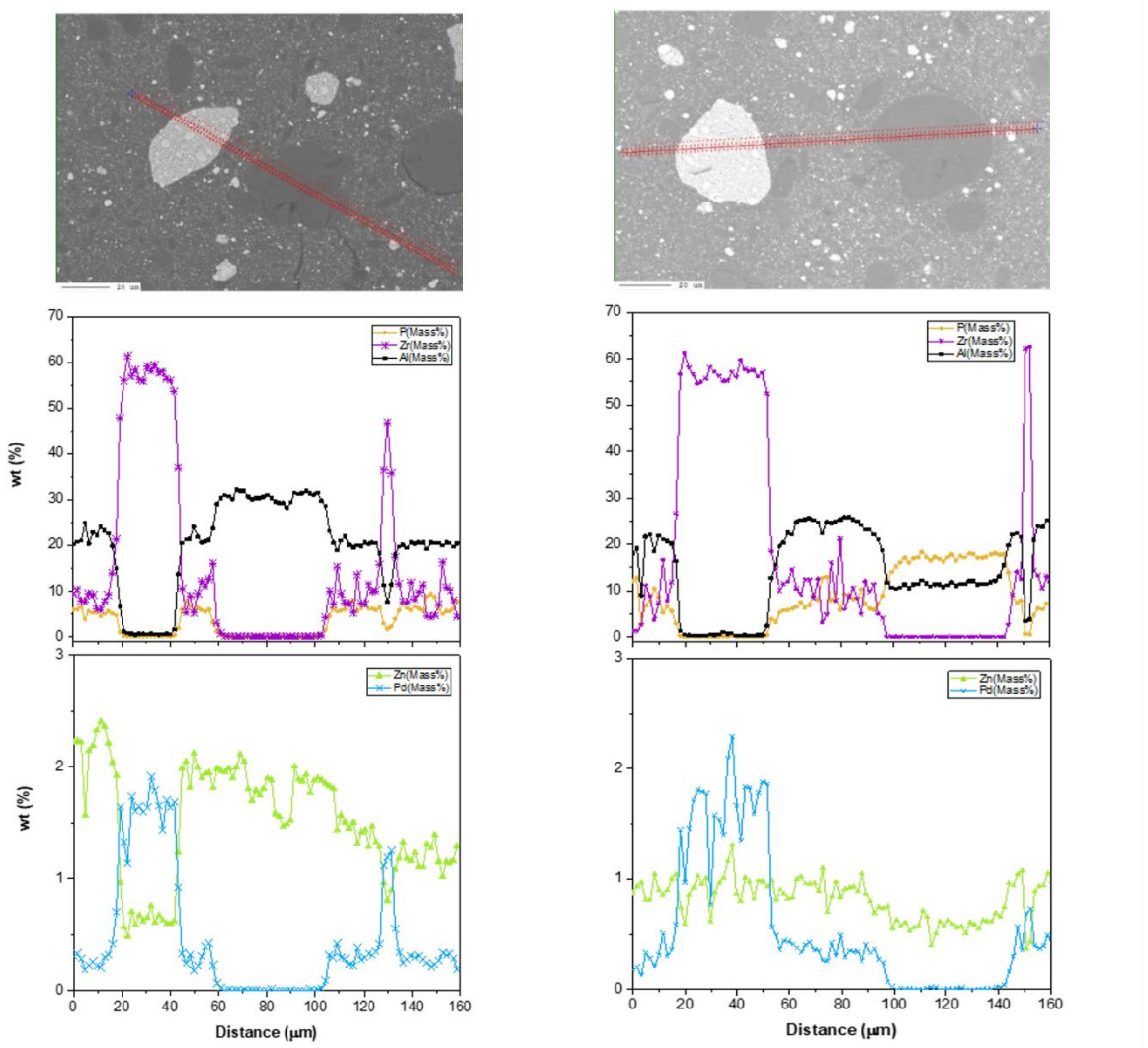

Figure 5. $PdZn/ZrO_2$ + SAPO-34 extrudate element concentration profile. Reproduced from [6].

4 Kinetic modeling

The kinetic model for the tandem conversion of CO_2 to light hydrocarbons was developed by using the convection-dispersion-reaction equation for each compound in the reaction medium. Due to the reactor characteristics, isobaric and isothermal conditions were assumed (reactor diameter of 2 mm and less than 5 cm bed height). Moreover, pure convective transport was assumed, with negligible radial dispersion due to the small diameter of the reactor, and negligible axial dispersion, with Re values of ca. 10^5 at the used flow condition. Deactivation was not observed during long-time experiments and after the catalyst pretreatment in H_2 and the first hours of reaction, steady state was reached. With this assumption, the reactor can be modeled using the steady-state design equation for a packed bed reactor. Then, the molar fraction of each *i* compound (y_i) can be expressed as

$$\frac{1}{S}\frac{d\left(Fy_i\right)}{dz} = \rho\sum_j \nu_{ij}\, r_j \tag{1}$$

for a catalytic bed length $0 < z < L$, where S is the reactor cross-section, F is the total molar flow rate, ρ is the bed density, ν_{ij} is the stoichiometric coefficient of each i compound in each j step of the reaction network and r_j is the reaction rate of each j step of the reaction network, described by the reactions occurring through interaction with both functions of the catalyst: hydrogenation on the metal alloy/oxide and MTH chemistry on the SAPO-34:

$$CO_2 + 3H_2 \overset{1}{\rightleftharpoons} CH_3OH + H_2O \tag{2}$$

$$CO_2 + H_2 \overset{2}{\rightleftharpoons} CO + H_2O \tag{3}$$

$$CO + 2H_2 \overset{3}{\rightleftharpoons} CH_3OH \tag{4}$$

$$CO + 3H_2 \overset{4}{\longrightarrow} CH_4 + H_2O \tag{5}$$

$$2CH_3OH + H_2 \overset{5}{\longrightarrow} C_2H_6 + 2H_2O \tag{6}$$

$$3CH_3OH + H_2 \overset{6}{\longrightarrow} C_3H_8 + 3H_2O \tag{7}$$

$$4CH_3OH + H_2 \overset{7}{\longrightarrow} C_4H_{10} + 4H_2O \tag{8}$$

On the metal alloy/oxide function, the following reactions were considered: CO_2 hydrogenation to methanol (reaction 1, **Eq. 2**), reverse water-gas shift (reaction 2, **Eq. 3**), CO hydrogenation to methanol (reaction 3, **Eq. 4**) and the undesired formation of methane from CO (reaction 4, **Eq. 5**). On the other hand, methanol conversion to ethylene, propylene and butenes was assumed to proceed over the SAPO-34. Nevertheless, our previous observations suggest that the presence of high partial pressure of H_2 and this Pd-containing catalyst led to fast hydrogenation of unsaturated hydrocarbons to ethane, propane and butanes, thereby contributing to reactions 5-7 (**Eqs. 6-8**).

Reaction rates (r_j) are defined by Langmuir-Hinshelwood equations

$$r_1 = \frac{k_1\left(P_{CO_2}P_{H_2}{}^3 - \frac{P_{CH_3OH}P_{H_2O}}{K_1}\right)}{\left(1 + K_{CO_2}P_{CO_2} + \sqrt{K_{H_2}P_{H_2}}\right)^2} \tag{9}$$

$$r_2 = \frac{k_2\left(P_{CO_2}P_{H_2} - \frac{P_{CO}P_{H_2O}}{K_2}\right)}{\left(1 + K_{CO_2}P_{CO_2} + \sqrt{K_{H_2}P_{H_2}}\right)^2} \tag{10}$$

$$r_3 = \frac{k_3\left(P_{CO}P_{H_2}{}^2 - \frac{P_{CH_3OH}}{K_3}\right)}{\left(1 + K_{CO_2}P_{CO_2} + \sqrt{K_{H_2}P_{H_2}}\right)^2} \tag{11}$$

$$r_4 = \frac{k_4 P_{CO} P_{H_2}}{\left(1 + K_{CO_2} P_{CO_2} + \sqrt{K_{H_2} P_{H_2}}\right)^2} \quad (12)$$

$$r_5 = \frac{k_5 P_{CH_3OH}}{1 + K_{H_2O} P_{H_2O}} \quad (13)$$

$$r_6 = \frac{k_6 P_{CH_3OH}}{1 + K_{H_2O} P_{H_2O}} \quad (14)$$

$$r_7 = \frac{k_7 P_{CH_3OH}}{1 + K_{H_2O} P_{H_2O}} \quad (15)$$

where k_j is the kinetic constant of each j step of the reaction network (**Eqs. 2-8**), K_j is the equilibrium constant of each j step, P_i is the partial pressure of each i compound and K_i is the adsorption constant of each compound (CO_2, H_2 and water). For those hydrogenation reactions that take place on the metal alloy/oxide, the adsorption of CO_2 and the dissociative adsorption of H_2 were considered in a single site. The equilibria of the first three reactions are considered using the empirical correlations with temperature proposed by Iluita et al.[7] and kinetic constants (k_j) are defined with a reparameterized form of the Arrhenius equation

$$k_j = k_j^* \exp\left[-\frac{E_j}{R}\left(\frac{1}{T} - \frac{1}{T^*}\right)\right], \quad (16)$$

where k^*_j is the kinetic constant of each j step of the reaction network at the reference temperature T^* (623 K), E_j is the apparent activation energy of each j step of the reaction network and R is the universal gas constant.

The system of partial differential equations was transformed into a system of ordinary equations and solved using a finite-difference method discretization and a Runge-Kutta method of orders 1-5. The reactor model was solved by iterative computation to optimize the k^*_j, E_j and K_i parameters. For that, an objective function to be minimized was defined based on the sum of square errors (SSE) between calculated and experimental data

$$SSE = \sum_{i=1}^{n_c} \omega_i \sum_{n=1}^{n_e} \left(y_i - y_i^e\right)_n^2, \quad (17)$$

where y_i and y^e_i are the calculated and experimental molar fractions of each i compound, respectively, ω_i is the weight factor considered for each i compound and n_c and n_e are the number of compounds and experiments, respectively.

Figure 6a and **6b** show a comparison between calculated and experimental data under the most relevant operating conditions: 350 ºC and 30 bar (**Figure 6a**) or 40 bar (**Figure 6b**) for pure CO_2 feed (central point of the experimental design). As observed, the evolution with

[7] Iliuta et al., Dimethyl ether synthesis with in situ H_2O removal in fixed-bed membrane reactor: Model and simulations, *Ind. Eng. Chem. Res*., **2010**, 49, 6870–6877

space time of the C-containing products is well predicted by the model. In both cases, CO_2 simulated conversion match our experimental observations, and the main secondary product is CO. As representative of hydrocarbons, the C_3 fraction, which is most abundant, continuously increases with space time. An individual analysis of CO reactivity is required for the computation of CO hydrogenation to methanol (reaction 3, **Eq. 4**) and its mathematical decoupling from methanol formation *via* WGS (reverse reaction 2, **Eq. 3**) plus CO_2 to methanol (reaction 1, **Eq. 2**) reactions. As illustrated in **Figure 6c**, our model is also able to predict CO tandem hydrogenation to hydrocarbons at different conditions: CO/CO_2 co-feed at optimal process conditions (solid symbols and continuous line); CO hydrogenation at optimal process conditions (hollow symbols and dashed lines) and; CO hydrogenation at the harshest tested conditions (crossed symbols and double lines). In those experiments, the evolution with space time of CO conversion, CO_2 formation *via* WGS (reverse reaction 2, **Eq. 3**) and hydrocarbon formation *via hydrocarbon pool* is followed by the model.

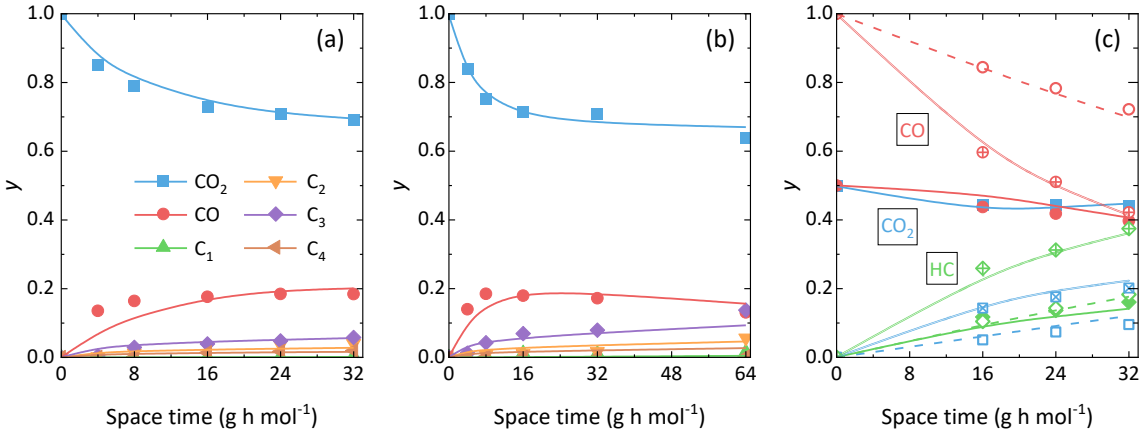

Figure 6. Comparison of experimental and calculated molar fractions (*y* on C basis) at 350 ºC and (a) 30 bar and (b) 40 bar for pure CO_2 feed. (c) Experimental data fitting with CO in the feed at selected conditions: CO_2:CO, 0.5:0.5, 350 ºC and 30 bar (solid symbols and continuous line); CO_2:CO, 0:1, 350 ºC and 30 bar (hollow symbols and dashed lines); CO_2:CO, 0:1, 400 ºC and 40 bar (crossed symbols and double lines). All data collected with CO_x:H_2 1:3. Reproduced from [8]

One of the most crucial variables in the process is the formation of water during the reaction. Water is formed from CO_2 hydrogenation, but also from methanol conversion to hydrocarbons and its concentration affects the thermodynamics of the reaction, strongly limiting reactions 1 and 2 of the kinetic network (**Eqs. 2** and **3**). The evolution of water with the catalytic bed length was simulated at different conditions and its concentration (in mol mol_C^{-1}) is depicted in **Figure 7a**. At 350 ºC and feeding pure CO_2 (red lines), water concentration shows an asymptotic trend towards 0.4 mol mol_C^{-1} when the reaction is carried out at 30 bar (dashed red line). At 40 bar, due to the evolution of CO_2 conversion, the model no longer predicts the asymptotic trend (solid lines). A maximum value of 0.5 mol mol_C^{-1} can be achieved

[8] Cordero-Lanzac et al., A CO_2 valorization plant to produce light hydrocarbons: kinetic model, process design and life cycle assessment. *Journal of CO_2 utilization*, **2023**, 67, 102337. DOI: 10.1016/j.jcou.2022.102337

when increasing the reaction temperature up to 400 ºC. This increase in the water concentration with temperature is explained by the promotion of MTH reactions at high temperature. The concentration of water in the reactor can be drastically decreased by co-feeding CO. Considering the asymptotic values at the outlet of the reactor operating at 30 bar (dashed lines), co-feeding 50% CO_2/CO decreases water concentration to 0.2 mol mol_C^{-1}, whereas reaction with pure CO produces a maximum water concentration of 0.05 mol mol_C^{-1}. Again, CO concentration in the feed stream could play an important role in the reaction medium, which should be considered without disregarding the main goal of CO_2 valorization.

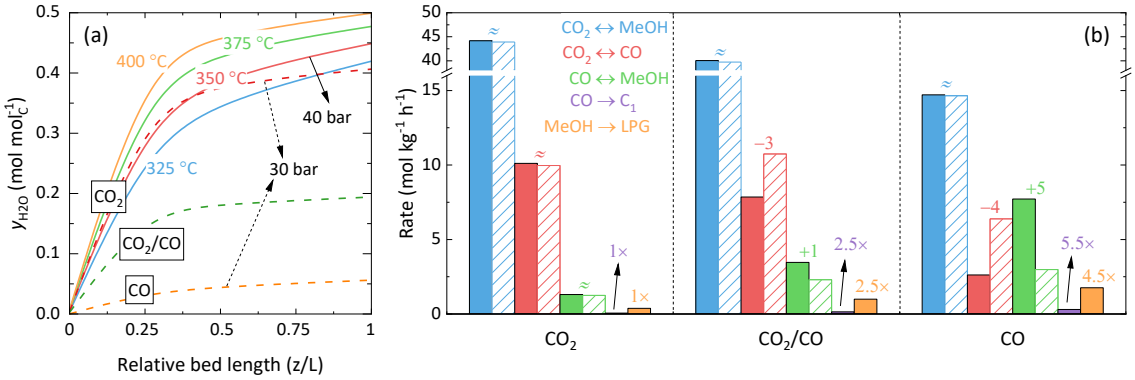

Figure 7. (a) Effect of temperature, total pressure and CO_2/CO feed concentration on the predicted water profile in the reactor and (b) influence of CO_2/CO feed concentration on the reaction rates at 350 ºC, 30 bar. All data computed for space time of 32 g h mol^{-1} (GHSV, 3000 cm^3 h^{-1} g^{-1}) and CO_x:H_2, 1:3. Reproduced from [8].

Further investigation on the kinetics for these three different feeds were performed. **Figure 7b** shows reaction rate values for all steps considered in the kinetic network (**Eqs. 2-8** and inset of **Figure 7b**). Reversible reaction rates are depicted with patterned white bars. At relevant space-time values and pure CO_2 feed, CO_2 hydrogenation to methanol, rWGS reaction and CO hydrogenation to methanol are in equilibrium, indicating the hard thermodynamic limitations of the process. These reactions, and especially those involving CO_2, are significantly faster than MTH chemistry at 350 ºC (apparent rate also considering hydrocarbon hydrogenation). The rate of CO_2 hydrogenation (reaction 1, blue in **Figure 7b**) decreases when co-feeding CO but forward and reverse rates are in equilibrium independently of the feed composition. Nonetheless, the presence of CO in the feed modifies rate distributions. WGS reaction (reverse reaction 2, **Eq. 3**) becomes relevant when increasing CO in the feed due to the presence of water in the reaction medium (**Figure 7a**), as well as the production of methanol through CO hydrogenation (forward reaction 3, **Eq. 4**). Consequently, the rate of LPG formation is boosted (up to 4.5 times, **Figure 7b**) but the valorization of CO_2 drops. This behavior is better observed following the evolution of CO and CO_2 concentration in the reactor when these two compounds are co-fed (solid symbols and continuous line **Figure 6c**). Close to the reactor entrance (low space time), both CO and CO_2 are consumed. However, when the concentration of water is higher and WGS reaction is triggered, CO conversion is boosted and CO_2 concentration increases, which should be avoided in order to maximize CO_2 valorization. Although the rate of LPG formation increases with CO feeds, the rate of undesired methane formation increases

even more (up to 5.5 times, **Figure 7b**). Methane should be avoided in the CO_2 valorization plant due to separation issues.

5 Conclusions

Among the tested combinations for the tandem hydrogenation of CO_2 to propane and propene, the $PdZn/ZrO_2$ + SAPO-34 catalyst combination was found to provide the highest CO_2 conversion (40%) and propane selectivity (50%, with 20% CO, 6% C_1, 13% C_2, 10% C_4, and 1% C_5). By means of X-Ray absorption spectroscopy (XAS) and transmission electron microscopy (TEM), we found that PdZn alloy formation was key for the high activity of this catalyst combination. Moreover, the intimately mixed $PdZn/ZrO_2$ and SAPO-34 components shifted the overall reaction equilibrium, boosting CO_2 conversion and minimizing CO selectivity. This catalyst combination was also able to transform CO into hydrocarbon, which can also play an important role in the industrial system where most of CO needs to be recirculated together with the unreacted CO_2 and H_2.

With this industrial perspective, different synthesis strategies were evaluated for the catalyst production at larger scale. The modification of the $PdZn/ZrO_2$ synthesis route from a colloidal impregnation to a simpler incipient wetness impregnation method provided a successful result in terms of catalytic performance, with 90% activity compared to the original catalyst. Characterization results demonstrated the formation of the PdZn alloy in this catalyst as well. Both catalytic functions, $PdZn/ZrO_2$ and SAPO-34, were also formulated together in tablet and extrudate shapes to obtain a more conventional industrial catalyst using Al-based binders. In these cases, we observed Zn migration from the ZrO_2 matrix to the Al binder and SAPO-34 surface, which decreased (tablets) or suppressed (extrudates) the activity of the catalyst. These catalysts, combining both functions in one shaped body, were discarded for further studies.

The physical mixture of the upscaled $PdZn/ZrO_2$ and SAPO-34 was then selected as first generation catalyst and a detailed kinetic study and model was developed with the obtained results. The model was able to predict the evolution of the reaction for CO_2 feeds, CO feeds and mixtures of both. The obtained kinetic parameters suggested the equilibrium limitation of the reactions taking place in the $PdZn/ZrO_2$ function (CO_2 and CO hydrogenation and water-gas shift reactions). The model was also able to predict the evolution of water during the reaction, one of the key components in the reaction medium affecting CO_2 hydrogenation and methanol-to-olefins chemistry.